ICES Journal of Marine Science, 57: 793–807. 2000
doi:jmsc.1999.0517, available online at http://www.idealibrary.com on IDEAL®

Review and recommendations for the modelling of acoustic scattering by fluid-like elongated zooplankton: euphausiids and copepods

Timothy K. Stanton and Dezhang Chu

Stanton, T. K. and Chu, D. 2000. Review and recommendations for the modelling of acoustic scattering by fluid-like elongated zooplankton: euphausiids and copepods. – ICES Journal of Marine Science, 57: 793–807.

Acoustic echo sounders are commonly used to survey zooplankton. An essential element in the methods is the acoustic scattering model, which relates acoustic echo data to meaningful biological parameters such as size and numerical density. Because of the importance of scattering models, there has been much development of models of increasing sophistication. With the increase in sophistication is an associated improvement in accuracy, but possibly at the cost of increased effort in implementing the model. Thus the practical question is which model provides sufficient accuracy for the scientific problem of interest. This paper presents a modelling study using a wide range of models, ranging from simple to complex representation of the animals, a synthesis of previously published laboratory scattering data from a variety of sources, and laboratory data presented for the first time. The focus is on fluid-like zooplankton (i.e., animals that do not support shear waves) with examples specific to euphausiids, shrimp, and copepods. The simplest model is the sphere with homogeneous material properties while the most complex is a high-resolution digitized form of each zooplankton taking into account surficial roughness and inhomogeneities of the material properties. The results show that there are conditions under which very simple, easy-to-use models can be used with reasonable accuracy while there are other conditions where the more complex models must be used.

Key words: acoustics, scattering, zooplankton, biomass.

Received 1 June 1999; accepted 6 September 1999.

Timothy K. Stanton and Dezhang Chu: Department of Applied Ocean Physics and Engineering, Woods Hole Oceanographic Institution, 98 Water Street, Woods Hole, Massachusetts 02543-1053, USA.

Introduction

Acoustic echo sounders have long been used to map distributions of zooplankton. The data provide high-resolution synoptic information regarding the spatial and temporal variability of the animals. In order to relate quantitatively the acoustic echoes to meaningful biological parameters such as length and numerical density, acoustic scattering models need to be used which describe the efficiency with which the animals scatter sound. The acoustic scattering process is a complex function of animal size, shape, orientation, and material properties as well as acoustic frequency or wavelength. Because of the complexity, development of the models has been a great challenge and has resulted in a number of models of varying accuracy and generality.

Much attention has been paid to acoustic scattering by euphausiids and copepods, given their abundance and relative importance to the biological and ecological communities. There has been an evolution of zooplankton scattering models of these animals beginning with the initial model of zooplankton as a homogeneous sphere, regardless of the animal shape (Anderson, 1950; Greenlaw, 1977, 1979; Johnson, 1977; Stanton *et al.*, 1987; Holliday *et al.*, 1989; Holliday and Pieper, 1995). Since the initial use of the sphere model, increasingly sophisticated approaches have been used in order to take into account the full complexity of the animals' shape and material properties. The shape and material property profiles have been accommodated, at least in part, through use of deformed cylinder models. These models, while assuming that the cross-section of the animal is circular, can describe to some extent the

1054–3139/00/040793+15 $30.00/0

bend, taper, and roughness of the body, as well as the variability of the material properties.

There have been a number of formulations and applications of the deformed cylinder model. Initially, an approach based upon the exact modal-series solution to the infinitely long cylinder was developed and applied to elongated zooplankton (Stanton, 1988, 1989a; Wiebe *et al.*, 1990; Chu *et al.*, 1992; Miyashita *et al.*, 1996). Although this modal-series-based deformed cylinder model showed an improvement over the sphere model, the approach was only valid for target orientations near broadside incidence. A study on the range of validity of this approach was presented by Partridge and Smith (1995). During this period, deformed cylinder approaches were also developed that were simpler to calculate but had more limited use. Various high-pass models representing extensions of that originally developed by Johnson (1977) for the sphere were based, in part, on asymptotic values of the modal-series-based deformed cylinder model and applied to zooplankton (Stanton, 1989b; Wiebe *et al.*, 1990; Cochrane *et al.*, 1994; Stanton *et al.*, 1994a). Ray-based deformed-cylinder models have also shown great utility in predicting the frequency dependence of the scattering for single pings, the statistics of ping-to-ping variability, as well as for average levels (Stanton *et al.*, 1993a,b, 1994a,b, 1996, 1998a; Cochrane *et al.*, 1994; Martin *et al.*, 1996; Martin Traykovski *et al.*, 1998a).

Most recently, the deformed cylinder model has been applied to zooplankton using the Distorted Wave Born Approximation (DWBA). This was first used in Chu *et al.* (1993) and Stanton *et al.* (1993b) and presented in explicit (deformed-cylinder) form in Stanton *et al.* (1998a). The DWBA-based deformed cylinder model is similar in form to the deformed-cylinder model presented in Stanton (1989a). Both involve integrating a scattering function or kernel along the length of the axis of the body while at the same time taking into account the phase shift due to the deformation of the axis (the exponential term). The main difference between the two is the scattering function in the integrand. The modal-series-based deformed cylinder approach is valid for a wide range of material properties, but is limited to angles of orientation of the object near broadside incidence. The function for the DWBA-based deformed cylinder model was derived under the assumption that the body is weakly scattering (i.e., it has material properties similar to that of the surrounding water). Although the restriction of the material properties in the DWBA-based deformed cylinder model limits the usefulness of the method with respect to material properties, it is valid for all angles of orientation. It therefore appears to be well-suited to a wide range of animals such as euphausiids, copepods, shrimp, salps, and the tissue portion of siphonophores (i.e., the portion that does not include the gas), since they all have material properties similar to that of water. Finally, although the applications of the DWBA-based approach have been limited to cylinder-based shapes, more general three-dimensional shapes can also be modelled with this approach. An alternative approach would be numerical modelling methods which have the advantage of allowing a wider range of material properties (Francis *et al.*, 1996; Foote, 1998).

Various shape or taper functions have been incorporated with the DWBA-based deformed cylinder model: the straight finite cylinder and the bent cylinder, each with rounded edges (Stanton *et al.*, 1993b, 1998b; Chu *et al.*, 1993), a deformed finite cylinder whose taper function matches the coarse body features of euphausiids (McGehee *et al.*, 1998; Martin Traykovski *et al.*, 1998b), and a deformed finite cylinder that takes into account the shape of the coarse body features as well as small features on the body and inhomogeneities of the material properties (Stanton *et al.*, 1998a).

Given the development of increasingly complex models and the fact that the models are now relatively mature, it is timely to review the various approaches, perform intercomparisons, and make recommendations as to the conditions under which the different approaches are valid. Certainly the most complex approach will tend to be valid under more conditions, however, there are simpler approaches that have merit by virtue of their ease of application under limited conditions.

In this paper the DWBA-based deformed cylinder model is used to predict acoustic scattering by euphausiids and copepods over a wide range of modelling parameters. These parameters include a range of shape and material property profiles so that the sensitivity of the scattering with respect to these different profiles can be determined. The modelling results are compared with each other as well as to simplified formulae and laboratory data. Recommendations are then made for the conditions under which the different models may be useful.

Modelling equations

Basic definitions

The scattering by a target can be described in terms of the incident sound pressure (P_0), the acoustic wave number (k_1) ($=2\pi/\lambda_1$ where λ_1 is the wavelength and the subscript 1 denotes the surrounding fluid), a distance (r) between the receiver and target, and scattering amplitude (f) as

$$p_{scat} = P_0 \frac{e^{ik_1 r}}{r} f, \tag{1}$$

Using this equation, the target strength (TS) of the target can be defined in terms of the square of the magnitude of the scattering amplitude in the backscatter direction as:

$$TS = 10\log|f_{bs}|^2 = 10\log\sigma_{bs} = 10\log(\sigma/4\pi), \quad (2)$$

where this expression is given in terms of the two backscattering cross-sections (σ_{bs} and σ) that appear in the literature (Urick, 1983; Medwin and Clay, 1998). The units of the target strength are dB relative to 1 m^2. In some cases, such as with bodies whose dimensions remain in the same proportions regardless of size, the target strength is scaled or normalized according to the square of an outer dimension of the body. The "reduced" target strength for elongated bodies is defined in terms of the target strength and length (L) of the body as:

$$RTS = TS - 10\log(L^2) \quad (3)$$

When averaging a set of echo data is involved, it is usual to average the backscattering cross-section which is related to echo energy. The "mean" target strength, which is related to the averaged level, is defined as:

$$\langle TS\rangle = 10\log\langle|f_{bs}|^2\rangle. \quad (4)$$

where the averaging is done before the logarithm is performed.

A general scattering approach

The animals of interest here have material properties (mass density and sound speed) that are to within several per cent of the surrounding water. Such objects with small contrasts in material properties are referred to as "weak scatterers". Furthermore, the shells are considered to be thin enough so that, to a good approximation, they can be assumed to be fluid-like in that they do not support shear waves. A general formulation that accurately describes the acoustic scattering by weakly scattering bodies is the DWBA given as (Morse and Ingard, 1968):

$$f_{bs} = \frac{k_1^2}{4\pi}\iiint_v (\gamma_\kappa - \gamma_\rho) e^{i2(\vec{k}_i)_2 \cdot \vec{r}_v} dv. \quad (5)$$

This approximate formula predicts the scattering by a body of arbitrary size, shape, orientation, and material properties (they can vary within the interior and be of any value provided they are similar to that of the surrounding fluid), as well as arbitrary frequency. The integration is within the volume (v) of the body with a position vector ($\vec{r}_v$) and using the incident wave number vector in the exponent evaluated inside the body ($[(\vec{k}_i)_2]$). The terms γ_κ and γ_ρ are related to the density and sound speed contrasts (g and h, respectively) of the body where $g = \rho_2/\rho_1$, $h = c_2/c_1$, ρ is the mass density, c is the sound speed, and the subscripts 1 and 2 refer to the surrounding fluid and body medium, respectively.

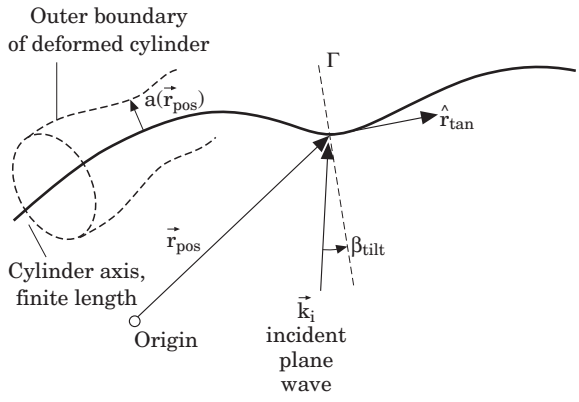

Figure 1. Scattering and integration geometry for DWBA-based deformed cylinder formulation.

Details of the equation are given in Morse and Ingard (1968) and Stanton *et al.* (1998a). The advantage of the equation is the fact that it is so general. However, the equation involves evaluating, either analytically or numerically, a three-dimensional integral which could make predictions of the scattering level a complex exercise.

Simplified scattering equations

Given the complexity of the above three-dimensional integral, it is attractive to consider alternate approaches that are more convenient to calculate, but still produce accurate results. Generally, the applicability of the approach becomes more restricted as the method becomes more simplified.

DWBA-based deformed cylinder model

Many elongated animals have a cross-section that can be approximated, to first order, as circular. With that restriction, and the assumption that the material properties only vary axially, the three-dimensional integral given above can be reduced analytically to the following one-dimensional integral that involves an integral along the axis of the body. This formulation, first used in Stanton *et al.* (1993b) and Chu *et al.* (1993) and presented in detail in Stanton *et al.* (1998a) is given as:

$$f_{bs} = \frac{k_1}{4}\int_{\vec{r}_{pos}} a(\gamma_\kappa - \gamma_\rho) e^{2i(\vec{k}_i)_2 \cdot \vec{r}_{pos}} \frac{J_1(2k_2 a\cos\beta_{tilt})}{\cos\beta_{tilt}} |d\vec{r}_{pos}|, \quad (6)$$

The term $\vec{r}_{pos}$ is the position vector of the body axis, J_1 is the Bessel function of the first kind of order one, k_2 is the acoustic wavenumber inside the body, and β_{tilt} is the angle between $\vec{k}_i$ and the thin disk or cross-section of the body at the point $\vec{r}_{pos}$ (Fig. 1). This deformed finite length cylinder formulation describes the scattering by finite length elongated bodies whose cross-sectional radius (a), radius of curvature, and material properties can vary along the axis of the body. This formula is valid

under the same wide range of conditions as the above, more general, three-dimensional approach, with the restrictions that the cross section of the body at each point along the axis must be circular and that the material properties are constant within a thin section at any given point (i.e., only vary axially).

Averaged ray solution

Applications in the natural environment may involve insonifying aggregations of animals spanning a range of sizes and orientations. Describing the scattering in that case involves performing an average of the scattering predictions from each individual. One approach would be to average numerically the results derived from one of the above formulae for each individual (Stanton *et al.*, 1993b). An alternative approach is to use a formula that has, through various simplifications, been analytically averaged. If the conditions are such that the approximations do not significantly compromise the quality of the predictions, then that approach would greatly simplify the process of making predictions.

A simple approximate formula has been derived to describe the scattering by an aggregation of elongated weakly scattering bodies whose lengths are narrowly distributed and whose angles of orientation (θ) can span an arbitrary range, provided that the range includes broadside incidence (Stanton *et al.*, 1993b). The formula is:

$$\langle |f_{bs}|^2 \rangle_{L,\theta} = 2A_{ij} R_{12}^2 \bar{a} \bar{L} \left[1 - e^{-8(k_2 \bar{a} s)^2} \cos(4k_2 \bar{a} + \mu_{p=2})\right], \quad k_1 a \geq 0.1, \quad (7)$$

where R_{12} is the plane-wave–plane-interface reflection coefficient of the body interface, $\bar{a}$ is the mean cylindrical radius, s is the standard deviation of the body length normalized by mean length ($\bar{L}$), and A_{ij} takes on different values for different combinations of shapes and orientation conditions (straight or bent cylinder; Gaussian or uniformly distributed orientation angle). For the case of uniformly bent cylinders whose orientation angle is Gaussian distributed, $A_{ij} = T_B^2 C_B^2 S_\theta / (16\, s_\theta \sqrt{\alpha_B})$, where T_B in this case is equal to unity, and C_B, S_θ, and α_B are approximately equal to 1.2, 1, and 0.8, respectively. The term s_θ is the standard deviation of orientation angle (in radians) and $\mu_{p=2} = -(\pi/2)\ k_1 a/(k_1 a + 0{\cdot}4)$. This formula is valid over the range of $k_1 a$ greater than 0.1 which, in essence, is the entire practical range of sizes and frequencies. This formula has been successfully compared with both numerical simulations, laboratory, and field data (Stanton *et al.*, 1993b, 1998a; Wiebe *et al.*, 1996).

Modelling parameters

As discussed above, acoustic scattering by the zooplankton is a complex function of animal size, shape, orientation, and material properties, as well as acoustic frequency (or equivalently, wavelength). In the modelling study described below, the parameters associated with these properties or quantities are varied over a wide range. In addition, the resolution or scale of certain parameters is varied. Specifically, the shape and material property profiles are varied from simple low-resolution models that are simple first-order approximations to the actual profile to more complex high-resolution models that contain fine features.

Size/frequency

The combination of size and frequency (i.e., $k_1 a$) is varied over the full range from small sizes and/or low frequencies (i.e., $k_1 a$ much less than unity) through large sizes and/or high frequencies (i.e., $k_1 a$ much greater than unity). Thus both the Rayleigh (low $k_1 a$) and geometric (high $k_1 a$) scattering regions are studied as well as the transition region between the two.

Digitizing the animal morphology

From an acoustic modelling perspective, the animal is a three-dimensional heterogeneity in an otherwise homogeneous medium. Incorporating the "heterogeneity" into an acoustic scattering model involves knowing the material properties, relative to that of the surrounding medium (water), as a function of position. Since there is generally no analytical formula to describe animal morphology, then it must be digitized according to measurements.

Digitizing the morphology of the animal should, in general, involve digitizing the material properties in three dimensions with a spatial resolution of a small fraction of the acoustic wavelength. This fraction should be roughly $\lambda/20$, but this condition may vary depending upon the type of scattering formulation used.

Although all information is obtained by digitizing the material properties in three dimensions, there is good reason to separate digitizing the morphology into two components: shape and material property variability within the outer boundary of the animal. A major reason is one of convenience. Given the extreme difficulty in digitizing small animals (animals that are sometimes smaller than 1 mm in length) in three dimensions, it is advantageous to find suitable approximations to the morphology. One approximation is to assume that the material properties are uniform inside the animal. The digitizing process is then reduced to measurements of the outer boundary of the animal as well as mean material property within the body. Another approximation is that the material properties within the body vary on scales larger than that of the variability of the outer surface. In that case, more information is required than for the case when the body is homogeneous, but less than for the case when full, high-resolution

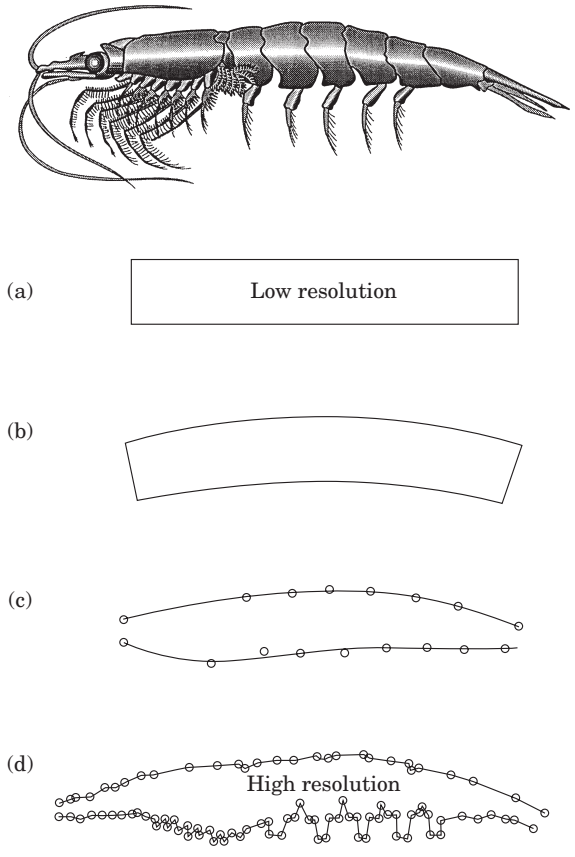

Figure 2. Euphausiid and various models of shape ranging from (a) low resolution to (d) high resolution. Euphausiid (*Meganyctiphanes norvegica*) illustration at top adapted from Wiebe (1976).

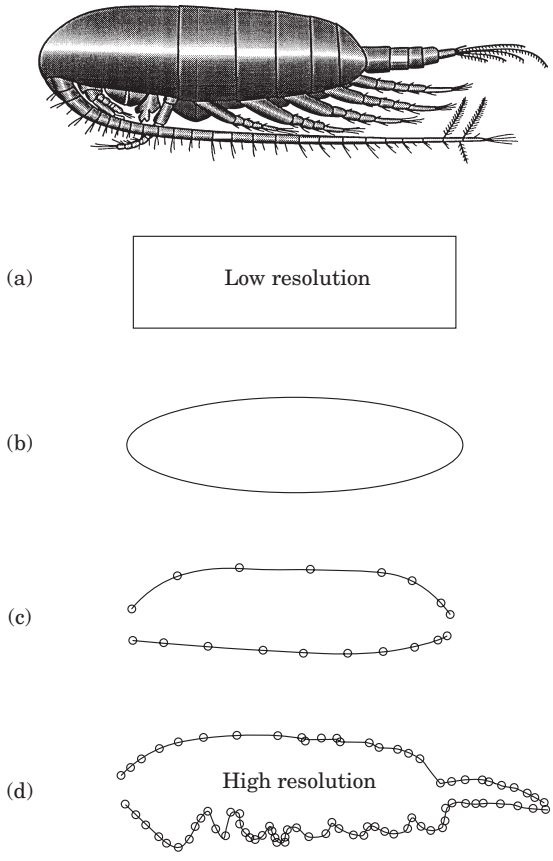

Figure 3. Copepod and various models of shape ranging from (a) low resolution to (d) high resolution. Copepod (*Calanus finmarchicus*) illustration at top adapted from Sars (1903).

three-dimensional digitizing is conducted. Finally, although there may be high variability of material properties within the animal, there may be conditions under which the variability does not significantly affect the acoustic signal (as per modelling illustrated later). For these latter conditions, it is recommended that the body be considered to be homogeneous so as to simplify digitization.

Specific issues regarding digitizing the shape and material properties within the body are discussed below.

Shape

The shape of the bodies of zooplankton is generally quite irregular (Figs 2 and 3). The challenge lies in both fully characterizing the shape as well as having a model that is general enough to be able to accommodate a realistic shape. Rigorous representation of the shapes of bodies sometimes requires taking into account all features of the order $\lambda/20$ and larger. For the purposes of this model intercomparison, the shapes of both a euphausiid and a copepod have been described with different degrees of resolution ranging from low resolution where the two animals are modelled as straight smooth finite cylinders, to high resolution where the bend of the body axis, tapering of the body, and local irregularities (legs, etc.) are taken into account. Clearly, the low-resolution model does not satisfy the ($\lambda/20$) resolution requirement stated above for very high frequencies. Nonetheless, the studies described below indicate the conditions under which it will provide reasonable results.

Material properties

There are very few data regarding material properties of the animals. The literature includes studies involving direct measurements of material properties with both dead and living animals as well as inferences of those properties based upon scattering measurements (assuming a perfect scattering model). The published values of the density and sound speed contrasts, g and h, are generally to within 1–2% of 1.04 for each value. Most studies to date have produced values of the average or bulk material property (i.e., assuming that the body was homogeneous) although there have been

some investigations of the structure of the animals' interior (Yayanos *et al.*, 1978; Foote, 1998). For example, Yayanos *et al.* (1978) observed that densities of lipids, which are composed mostly of wax esters, are a strong function of temperature. The acoustic scattering properties of lipid-bearing animals would then be a function of lipid content and temperature.

There are two key issues regarding the material properties, the overall average level as well as the degree of variability of the properties (inhomogeneities) within the body. Since the material properties of this class of animal are so close to that of the surrounding water (to within several per cent), a slight change in the contrast in properties relative to the water will result in a dramatic change in the acoustic scattering level. Similarly, for a slight uncertainty in material property, there can be a significant error in the predictions. This sensitivity has been documented in many previous studies and will be only briefly examined in the study below by making predictions over a range of properties. Because of the general lack of published data available involving the heterogeneities of the material properties, there must be a degree of speculation. Certainly, there is anatomical structure within the interior of the body of the animals. There will subsequently be scattering by the water–outer-boundary interface of the animals as well as by internal interfaces. Assuming that the internal structure corresponds to a variability in density and sound speed, a set of material property profiles has been constructed for the scattering predictions. Given the general lack of information available on the properties, the set of profiles was constructed in a systematic progression of increasing detail ranging from homogeneous to continuously varying (Fig. 4). The seven-segment profile was based on the fact that some animals have seven segments. Note that internal structure such as lipids also contribute to variability in the radial direction. This phenomenon is beyond the scope of the current study.

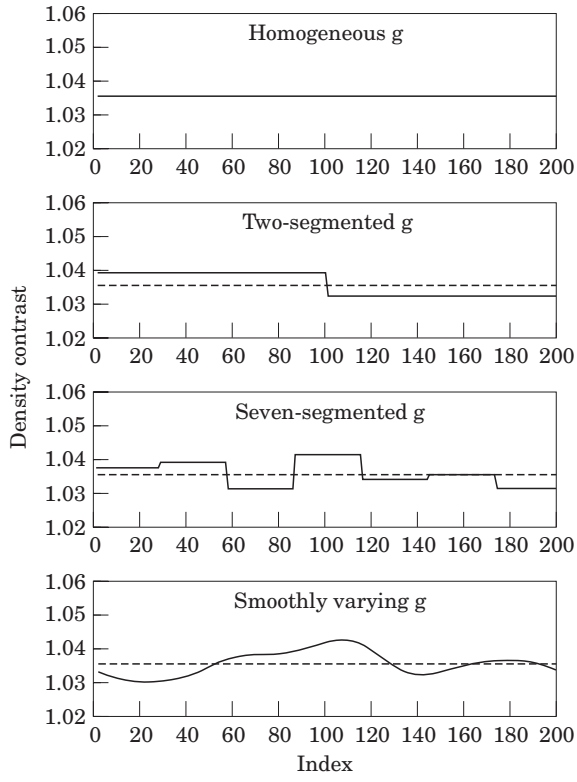

Figure 4. Models of material property profile along the length of an animal, ranging from uniform composition (top) to continuously variable (bottom). Given the lack of information to construct a realistic profile, these profiles are used in modelling exercises intended to span a range of possible profiles. Both density and sound speed contrast were modelled using the profiles given in these plots (solid), but with different mean values. The mean value of g is shown by the dashed line. The standard deviations of g and h about their mean values is 0.1ε, where the mean values of g or h are equal to $1+\varepsilon$ and ε takes on a different value for g and h.

Orientation

Very little information is available regarding the orientation distribution of free-swimming animals in the natural environment. There have been some investigations of krill in aquaria (Kils, 1981; Endo, 1993; Miyashita *et al.*, 1996) where the animals had mean orientations in the range of about 20 to 40° relative to horizontal (where 0° corresponds to a horizontal body axis and positive angles refer to the head up) with standard deviations of approximately 20°. Chu *et al.* (1993) applied a DWBA-based model to two-frequency data to infer the orientation parameters of encaged krill and estimated the mean orientation to be about 20°. Recently Benfield *et al.* (2000) reported the orientation distribution of copepods freely swimming over Georges Bank to be peaked at about 90° (i.e., the animal body axis was vertical with the head up) with a standard deviation of about 30°. Given the basic lack of information on orientation distributions, all orientation angles are investigated.

Simulations and model intercomparisons

All simulations in this section make use of the DWBA-based deformed cylinder model given in Equation (6), the shapes illustrated in Figures 2 and 3, and the material property profiles in Figure 4. The simulations illustrated in Figures 5–10 correspond to animals of typical lengths, a 30 mm long euphausiid and 3 mm long copepod. These distances actually represent the lengths of the lower resolution profiles given in Figure 2(a)–(c) and Figures 3(a)–(c), respectively. The lengths of the high-resolution profiles and actual animals are slightly longer as shown in Figures 2 and 3.

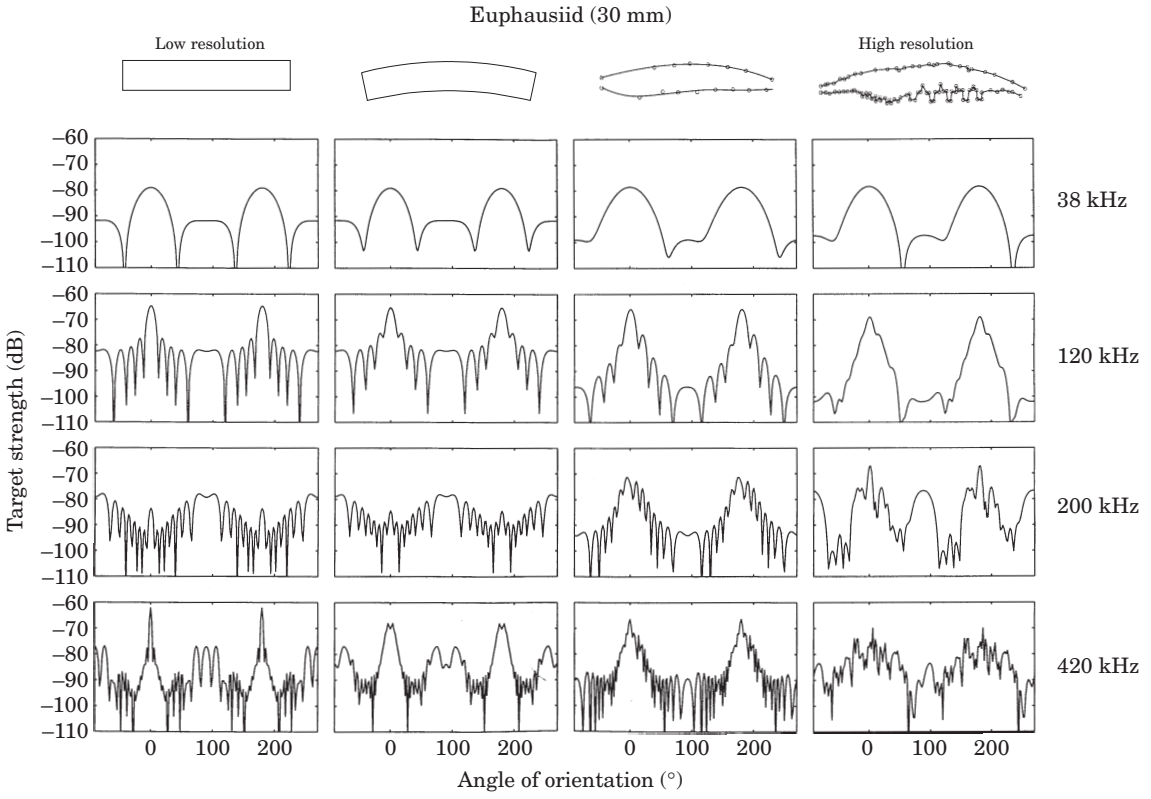

Figure 5. Target strength vs. angle of orientation for individual 30-mm-long euphausiid. The animal is modelled after four different deformed finite cylinders, taken directly from Figure 2, ranging from low resolution to high resolution: straight cylinder, uniformly bent cylinder, smooth tapered bent cylinder, and rough tapered bent cylinder. The predictions using the DWBA-based deformed cylinder formulation, involve four commonly used frequencies: 38, 120, 200, and 420 kHz. The material properties are uniform in each case with (g, h)=(1.0357, 1.0279) (Foote, 1990; Foote *et al.*, 1990). The radius of each cylinder for the simulations in the left two columns is a=2.3 mm. 0° is broadside incidence (dorsal aspect).

A major approximation in this cylinder-based approach is the assumption that the animals have a circular cross-section with material properties that only vary axially. In order to describe the profiles that were asymmetrically rough, the diameter at each point was set equal to the dorsal–ventral distance of the body at that point. The centre of the differential element (thin disk) followed an irregular path along the length of the body because of the surficial roughness. With this approach, the side view of the digitized body bore a resemblance of the actual shape. However, a top view would show unrealistic roughness on the sides of the body, especially for the high-resolution profiles. The facets created in this process significantly increased the scattering levels for angles of orientation near end-on incidence. In order to eliminate these artifacts, the high-resolution profiles and axes were smoothed slightly (not shown). In addition, although the material properties are modelled to vary axially, they also vary radially in animals. Certainly, a more rigorous approach would be to use the full three-dimensional representation of roughness and material profile with Equation (5). However, for the purpose of this investigation of exploring general effects and general conditions under which roughness and variability of material properties are important, the above-mentioned simplifications are made.

Shape and orientation dependence: various fixed frequencies

The scattering predictions show a very strong dependence upon shape, orientation, and frequency for both the euphausiid and copepod (Figs 5–7). The majority of the plots show a distinct peak in the scattering near broadside incidence. One exception to this involved the 200-kHz euphausiid simulations where k_1a was near 2 (i.e., in the presence of a null). There is variability in the peak value of the scattering from simulation to simulation. There is also variability in the ratio of peak value near broadside incidence to average level of side lobe near end-on incidence. Generally, the ratio of peak value to average side lobe level was lower for the straight, bent, and rough tapered bent cylinders;

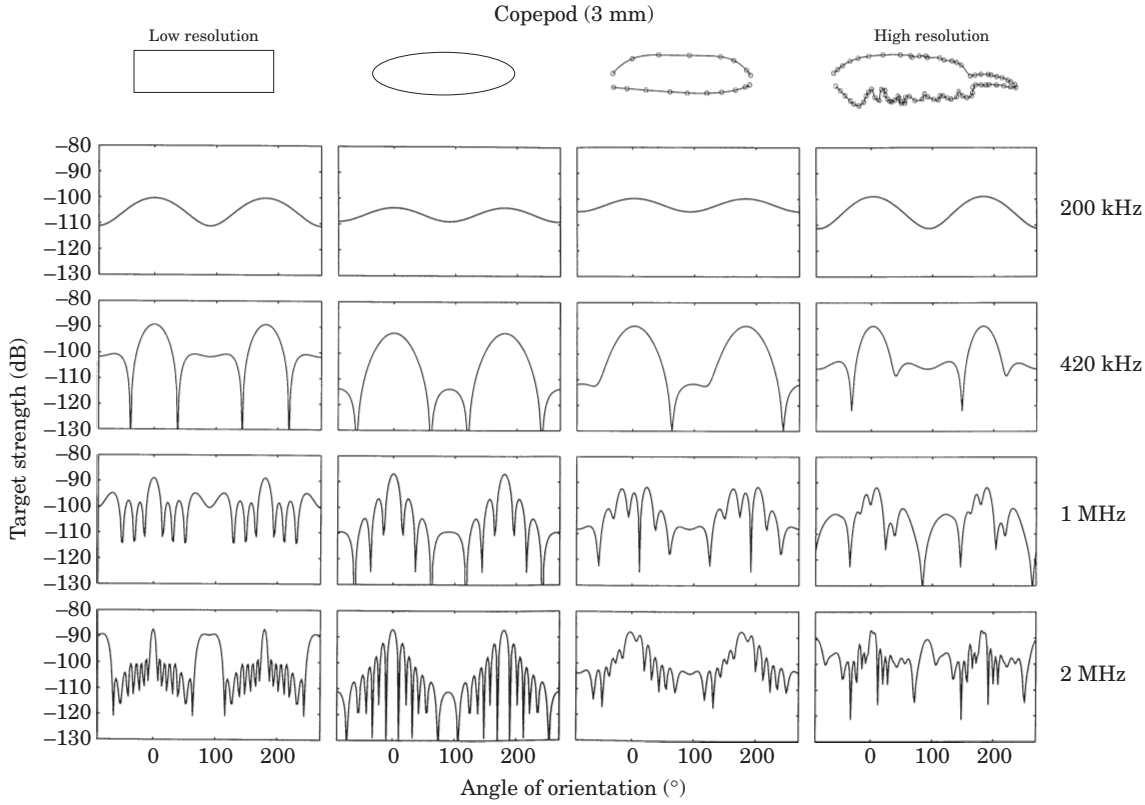

Figure 6. Target strength vs. angle of orientation for individual 3-mm-long copepod. The animal is modelled after four different deformed finite cylinders, taken directly from Figure 3, ranging from low resolution to high resolution: straight cylinder, prolate spheroid, smooth tapered bent cylinder, and rough tapered bent cylinder. The predictions, using the DWBA-based deformed cylinder formulation, involve four frequencies, the lower two of which are commonly used; 200 kHz, 420 kHz, 1 MHz, and 2 MHz. The material properties are uniform in each case using the euphausiid parameters given in Figure 5. The radius of the cylinder and length of the semi-minor axis of the prolate spheroid in the first two columns is 0.40 mm. 0° is broadside incidence (dorsal aspect).

and higher for the smooth tapered bent cylinder and prolate spheroid. Also, for the high-resolution model, the sidelobe values (i.e., values well off broadside) tend to increase with increasing frequency.

Material property dependence

Simulations were conducted first for a wide range of material properties for homogeneous bodies, then for a fixed mean value of material properties while varying the profile of the inhomogeneities.

Range of homogeneous properties

Simulations were performed for the rough tapered bent cylinder as a function of angle of orientation for one frequency over a range of material properties (Fig. 8). The range spanned that published for euphausiids and copepods. The results show the large change (of order 15 dB) in overall levels of scattering when the contrasts are varied from 1 to 6%.

Range of profiles of inhomogeneities

Simulations were conducted for the range of profiles of inhomogeneities shown in Figure 4 (Fig. 9). The axial variations tended to have the most effect in the sidelobe region (typically by raising the levels), especially when the sidelobes were initially low with a homogeneous profile. The inhomogeneities typically raised sidelobes by several dB, but in some cases by more.

Echoes averaged over orientation

The backscattering cross-sections for euphausiids were averaged over a distribution of angle and a narrow distribution of length (Fig. 10). The distribution of length represents either a single size class of animals that had a slight spread in sizes or it can represent a size bin

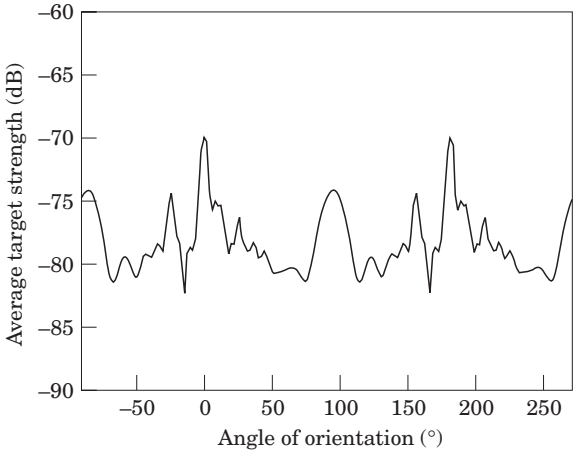

Figure 7. Target strength versus angle of orientation, averaged over band of frequencies, for individual 30 mm-long euphausiid. This simulation is designed to study total energy backscattered using a broadband acoustic system. Predictions using high-resolution (rough cylinder) taper function from Figure 2(d). The target strength is averaged first on a linear scale over the frequency range 350–600 kHz before the logarithm is taken. The material properties are uniform using the parameters given in Figure 5. 0° is broadside incidence (dorsal aspect).

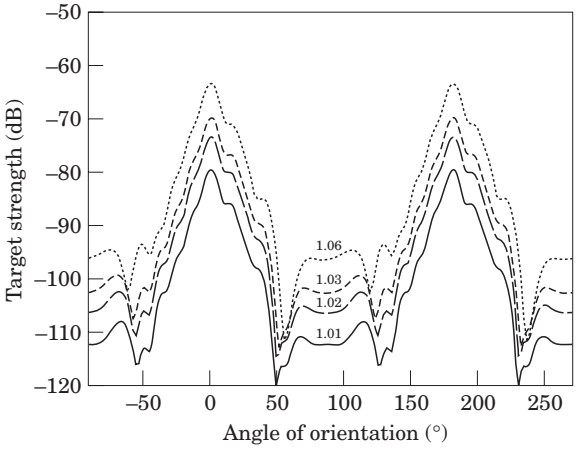

Figure 8. Effects of variation of homogeneous material properties of zooplankton on its target strength. Target strength is plotted as a function of angle of orientation for a 30 mm-long euphausiid at 120 kHz. The rough bent tapered cylinder shape profile from Figure 2(d) is used. Four different sets of density and sound speed contrasts are used: $g=h=1+\varepsilon$ where $\varepsilon=0.01$, 0.02, 0.03, and 0.06 for the different sets. 0° is broadside incidence (dorsal aspect).

in an otherwise broad distribution of sizes. The predictions used the four models of shape, ranging from low to high resolution.

For this distribution of angle centred near broadside, all patterns of averaged scattering follow a broadly similar trend of a rise in levels for k_1a less than unity and eventually levelling off for high values of k_1a. All plots have an oscillatory pattern for values of k_1a between 1 and 5. The peak values are to within about 1–2 dB of each other for the different plots and the high k_1a limit is also about the same for all plots. The dips near $k_1a=2$ and $k_1a=3.7$ are deeper for the straight and uniformly bent cylinders.

For distributions of angle centred well off broadside incidence, the straight and uniformly bent cylinder predictions are similar to each other while there is significant variability between the plots of the other shapes (plots not shown). The smooth tapered bent cylinder tends to have the lowest values.

Comparisons with laboratory data

The models are now compared with laboratory data, most of which have been presented in other papers. Two sets of phenomena are examined: variation of averaged echo levels with frequency and end-on incidence levels relative to peak or broadside levels.

Average echoes

Two sets of laboratory data are examined, one involving live tethered decapod shrimp (Stanton *et al.*, 1993b) and the other involving live free-swimming copepods presented here for the first time. Both sets of data were collected by the same acoustic scattering equipment at the Woods Hole Oceanographic Institution in 1992. The frequencies in both experiments spanned the range of the Rayleigh scattering region through the geometric scattering region. In the experiment involving the shrimp, up to 12 2-cm-long shrimp were insonified at a time in a 3.6-m-long tank filled with seawater over 50 kHz to 1.2 MHz. The animals were freely rotating about on tethers over the many pings collected, resulting in a uniform distribution of angles (0–360°). In the experiment involving the copepods, hundreds of 1-mm-long animals were freely swimming in the (horizontally aimed) acoustic beam at a time. Since the animals were freely swimming, a small aquarium was used to confine the animals and a vertical beam of light was used to attract them into the acoustic beam. The animals swam vertically towards the light, resulting in angles of incidence centred near normal incidence. A video camera was used to monitor numerical density and swimming direction. The range of frequencies, 500 kHz to 3 MHz, was used in the copepod experiments. In both experiments, the data from hundreds of pings were averaged to produce ensemble averaged levels.

Both simple and more complex models are compared with the data sets (Figs 11 and 12). The smooth tapered bent cylinder model, as calculated using the DWBA, is compared with the shrimp data as well as the simple ray-based bent cylinder formula presented in the original

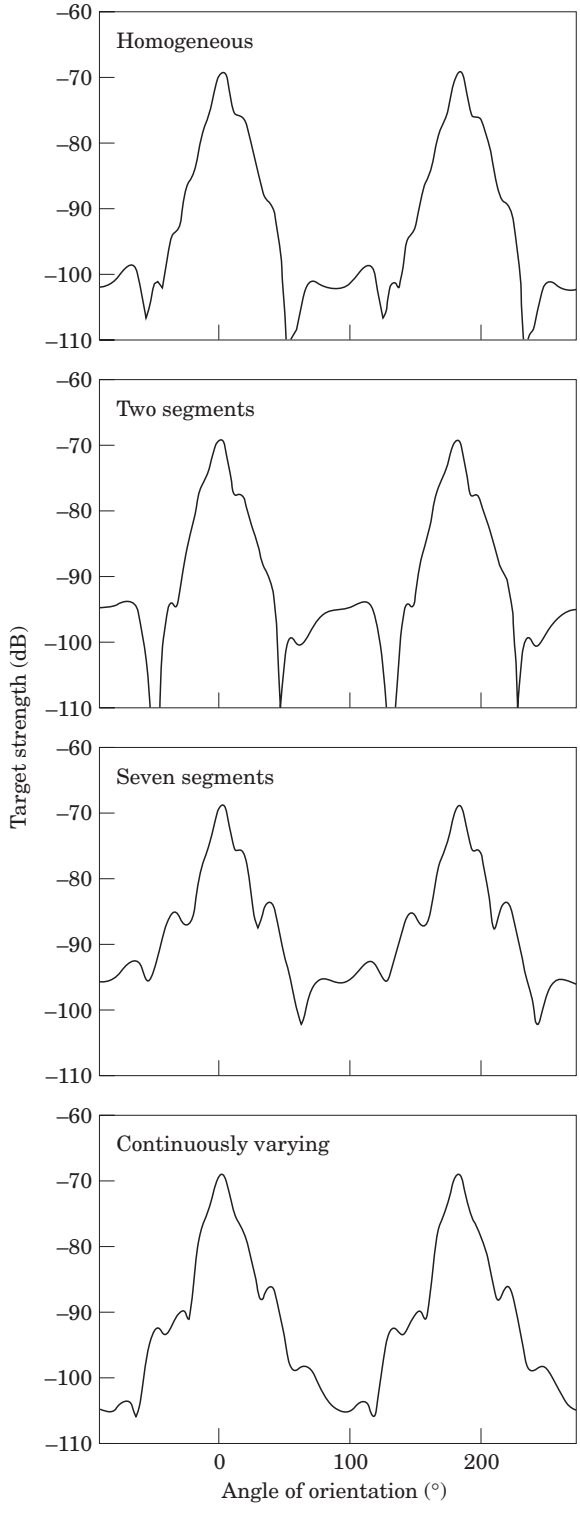

analysis. For the copepod data, the smooth prolate spheroid model, as calculated using the DWBA, is used as well as the exact solution to a sphere of the same volume as the animals. The sphere solution was used for comparison given the many studies published in the past that have used spheres as a basis for modelling.

The data for both types of animals show a rapid rise in the scattering levels at the lower frequencies and a tendency towards levelling off at the higher frequencies. There is some structure in each set of data near the Rayleigh/geometric transition region above $k_1a=1$. There are oscillations of the order of 5 and 2 dB in the shrimp and copepod data, respectively. The models predict structure in the Rayleigh/geometric transition region, although structure in some models is more pronounced than that occurring in the data. There is clearly much more agreement between those models that involve an elongated shape (i.e., resembling that of the animal) than those that involve a spherical shape. It is also clear that for these particular orientation distributions, the most complex models are not required.

End-on incidence

There are a number of sets of data in the literature involving measurements of backscatter vs. angle of orientation for various single frequencies or bands of frequencies. The angular dependence of the scattering is very dependent upon shape (e.g., roughness and degree of bend). Since the shape was not well documented in most of the papers, a direct comparison between the patterns of data and predictions of backscatter vs. angle would not be particularly useful. The predictions for the high resolution profiles show that the overall levels of the near-end-on scattering side lobes generally increase with frequency relative to the main scattering lobe. Since a comprehensive study on this topic has not yet been conducted, the overall levels of end-on incidence with respect to the peak levels from a variety of studies are examined (Table 1, Fig. 13). Given the variability in shape from species to species in those studies, the comparison is purely qualitative.

The data from the various sources show that the values of scattering near end-on incidence were generally higher relative to the peak values near broadside incidence for the higher frequencies. The values of end-on incidence scattering are roughly 5–20 dB below that of

Figure 9. Effects of different material property profile of zooplankton on its target strength. The axial variations from Figure 4 are used. Target strength for 30 mm-long euphausiid is plotted as a function of angle of orientation at 120 kHz. The rough bent tapered cylinder shape profile from Figure 2(d) is used. The average material properties are the same for each case: (g,h)=(1.0357, 1.0279). 0° is broadside incidence (dorsal aspect).

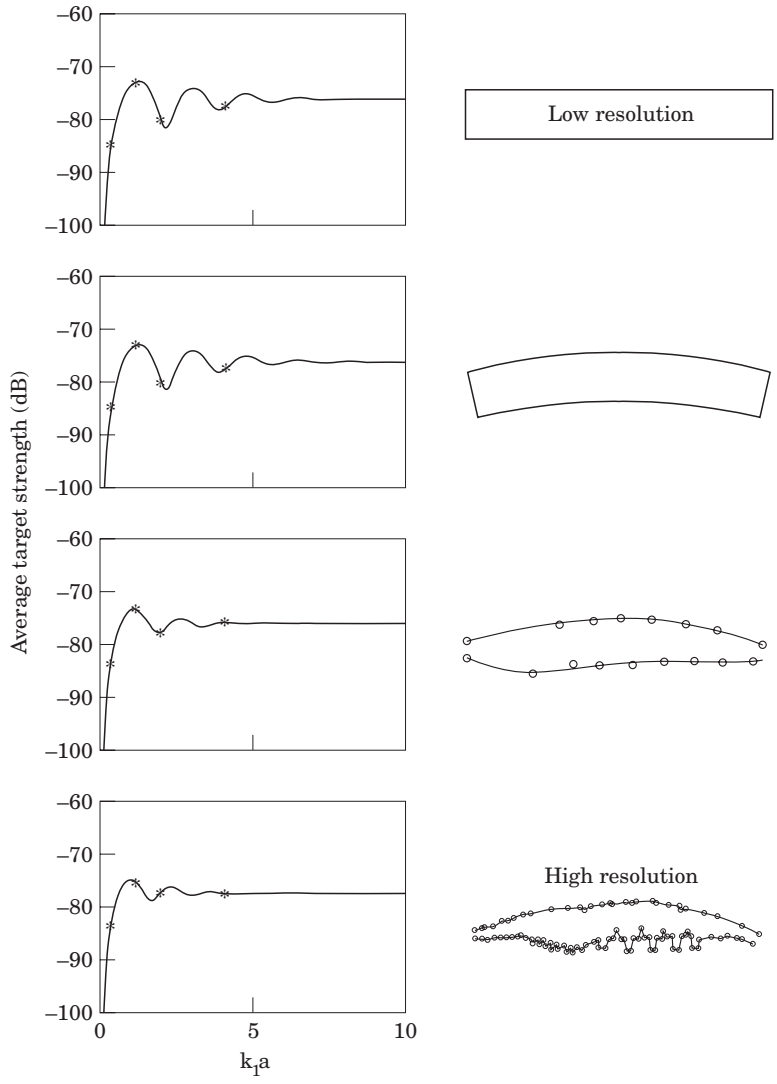

Figure 10. Target strength of 30 mm long euphausiid averaged over an orientation distribution involving near broadside incidence, N (20°, 20°) as well as for a narrow distribution of length (standard deviation of 10%). The averages are performed on a linear scale and are plotted vs. k_1a. The four shapes from Figure 2 spanning low to high resolution are used. The material properties are uniform using the parameters given in Figure 5. The radius of the cylinders in the top two plots is a = 2.3 mm. 0° is broadside incidence (dorsal aspect) and the positive angles are head up (toward a down-looking acoustic sysem).

the peak values of scattering for lower values of L/λ_1, and about 5–10 dB below the peak values for the higher values of L/λ_1.

Discussion

Depending upon the application, some of the predictions were more sensitive to the particular shape than others. For example, the pattern of backscattering vs. angle of orientation at a fixed frequency is strongly dependent upon shape. Furthermore, averages of echoes over orientations that were well away from broadside incidence (e.g., those including end-on incidence) were also strongly dependent upon shape. However, in the cases where broadside incidence angles were included in the averages, the predictions were relatively insensitive to shape. Regarding material properties, the well-known fact that the scattering was strongly dependent upon choice of average material properties was summarized in this study. Finally, it was shown that the degree of variability of material properties also influenced the scattering under certain conditions (axial variations altered scattering near end-on incidence).

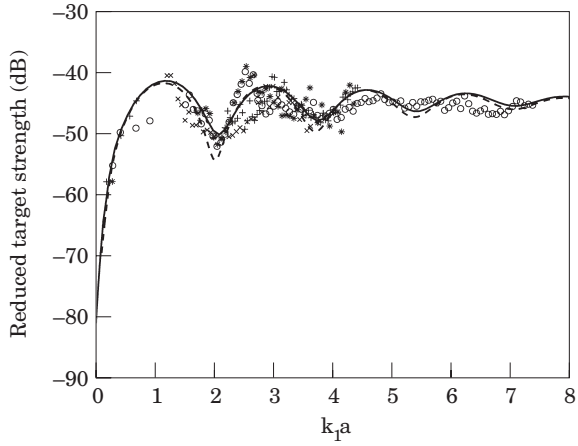

Figure 11. Comparison between two models and laboratory data involving decapod shrimp (*Palaemonetes vulgaris*). The laboratory data involve averaged echoes from up to 12 live tethered shrimp at a time in the beam. The animals were approximately 20 mm in length as measured from the anterior of the eye to the tip of the telson. The animals had orientations that spanned the full range, 0–360°, over the course of the experiment. One set of predictions involved calculations using the DWBA-based deformed finite cylinder model, which incorporated the shape of the smooth bent tapered cylinder from Figure 2(c) (solid line). These predictions involved numerical averages over size and orientation. The other set of predictions involved the use of the simple two-ray model using the shape of the uniformly bent cylinder from Figure 2(b), but slightly less bent. The ray model was analytically averaged over orientation and size [Equation (7)] (dashed line). Data and simulation parameters for both models from Stanton *et al.* (1993b).

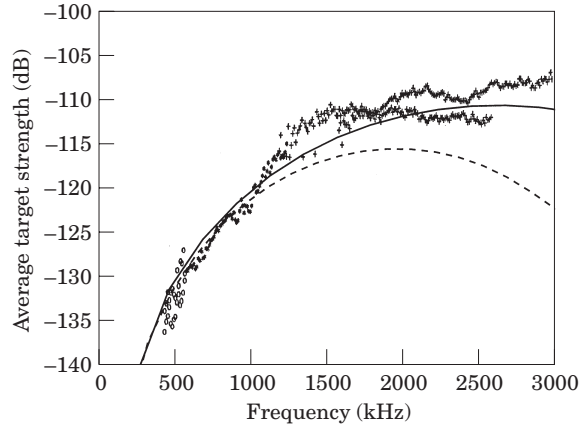

Figure 12. Comparison between two models and laboratory data involving copepods (*Pseudodiaptomus coronatus*). The laboratory data involve averaged echoes from hundreds of live (cultured) copepods that were freely swimming in the acoustic beam. The target strengths were calculated using the measured volume scattering strength and numerical density. The animals were approximately 0.94 mm in length (total length) with a 0.65-mm-long cephalothorax. A beam of light was used to attract the animals into the acoustic beam and, as a result, the copepods had a preferred direction of swimming of either towards the light (in the middle of the light beam) or away from the light (outside the boundary of the light beam). The copepods were observed with a video camera throughout the experiment. Because of the strong preference in the swimming direction, the average orientation of the animals in the acoustic beam is assumed to be normal incidence with a narrow distribution. One set of predictions involves calculations using the DWBA-based deformed finite cylinder model, using the smooth prolate spheroid shape from Figure 3(b) and a distribution of angles N (0°, 10°) (solid line). The measured cephalothorax length (0.650 mm) and body width (0.234 mm) were used for the dimensions of the prolate spheroid. The other set of predictions involves use of the exact solution to the sphere from Anderson (1950) (dashed line). Both sets of predictions used inferred values of g=h=1.01 (homogeneous) and an average over the measured distribution of lengths (standard deviation=10%).

Clearly, the rigorous way to approach this or any scattering predictions involving complex bodies is to digitize the shape and material properties of the object in increments much smaller than a wavelength (of order λ/20). Assuming that the scattering model is valid, use of such a digitized body will produce reliable results over the full range of conditions (all sizes, shapes, material properties, angles of orientation, and acoustic frequencies). However, the challenge arises when it is not possible to digitize all properties of the animal to a fine enough degree. This is especially true with small animals such as zooplankton. Thus, studies such as this provide information on the conditions under which the requirements can be reduced.

The studies show that when single pings are being investigated, the shape and material properties profile must be known with a high degree of precision. Furthermore, for volume scattering studies, high-resolution information must be used for the case when the acoustic beam is aimed vertically and the animals are generally well off broadside (such as in the case for copepods as observed by Benfield *et al.* (2000)). Once the echoes are averaged, there are conditions under which less precision is required. For example, averages involving distributions of angles including broadside are not particularly sensitive to precision of shape and axial material profile. This is because of the fact that the scattering is dominated by the echoes from the front and back interfaces of the animals near broadside. Errors due to an imperfect representation of the shape and material profile can become negligible once averaged with the large echoes from the interfaces. This is demonstrated by the fact that all models (DWBA-based and simple ray-based) were in general agreement with each other (with some differences in structure). However, for angles excluding broadside incidence, the echoes from the front and back interfaces are not part of the average and other effects will determine the scattering level. The scattering well away from broadside incidence is determined, to a large part, by the scattering off of roughness elements. Scattering by inhomogeneities can also play a role.

Table 1. Range of values of ratio of observed peak scattering value (near broadside) to observed echo levels near end-on incidence. Data taken from references, as indicated, where continuous line plots of TS vs. angle of orientation were available.

Reference	Species	Live/dead	Length (mm)	Frequency (kHz)	L/λ_1	$TS_{peak} - TS_{end\text{-}on}$ [range of differences (dB)]
1. Samovol'kin (1980)	Freshwater shrimp (species name not given)	Live	42	50	1.4	15 to 19
			42	120	3.4	5 to 17
2. Kristensen and Dalen (1986)	*Meganyctiphanes norvegica* (euphausiid)	Dead	43	40	1.1	5 to 14
			43	80	2.3	5 to 18
			43	315	9.0	3 to 8
3. Johnson (1993)	*Palaemonetes vulgaris* (decapod shrimp)	Live	30.1	72	1.4	8 to 15
			30.1	125	2.5	8 to 20
			30.1	167	3.4	8 to 14
			27.1	200	3.6	8 to 15
			30.0	350	7.0	5 to 9
			30.0	400	8.0	7 to 9
			30.0	450	9.0	6 to 10
			28.2	525	10.0	7 to 11
4. Stanton *et al.* (1998a)	*Meganyctiphanes norvegica* (euphausiid)	Live	36	350–600 (band average)	11	9 to 12
5. McGehee *et al.* (1998)	*Euphausia superba* (euphausiid)	Live	38	120	3.0	13 to 23
			42	120	3.4	10 to 17

It is apparent from these studies and the limited knowledge about the orientation distributions of zooplankton in their natural environment that some conditions can allow a simplified model while others will require the more complex rigorous models. The simpler models can be used for measurements of volume scattering strength (i.e., averaged echoes or "integrated echoes") and scattering geometries such as when the acoustic system is aimed in the vertical direction and the animals are swimming in a near-horizontal orientation. Also, the simpler models can be used (again for volume scattering strength) when the acoustic systems are aimed in the horizontal direction. In this latter case, the animals will tend to be randomly and uniformly oriented (0–360°) with respect to the system, unless they are migrating.

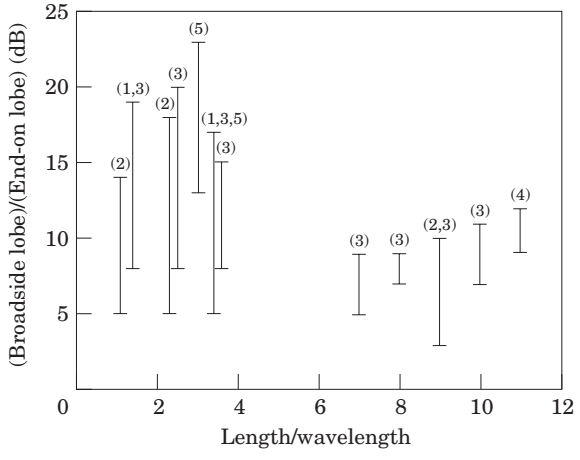

Figure 13. Difference, in dB, between peak scattering value near broadside incidence and side lobe level near end-on incidence from published measurements of backscatter vs. angle for various zooplankton. Given the variability of level of the end-on side lobes, the range of the differences is presented based upon the maximum and minimum value of the side lobes. There is some error associated with the subjective nature of identifying local maxima in echo levels as well as with the graphical picks of the values. Number at top of data bar corresponds to source of data listed in Table 1.

Summary and conclusions

Acoustic scattering predictions have been made over a wide range of shape and material property profiles, ranging from simple low-resolution to complex high-resolution representations of the animals. The studies show that there are indeed conditions under which the simpler lower resolution models can be used. Those conditions involve volume scattering strength measurements (i.e., averaged echo levels from aggregations of animals) when the range of orientations of the animals includes broadside incidence. Here, the echoes from the front and back interfaces tend to dominate the scattering and finer features, such as roughness, are less significant. For other conditions, such as single-ping analysis from individual animals and volume scattering strength analysis when the orientations do not include broadside (such as a vertically aimed echo sounder observing vertically

oriented copepods), the more complex models must be used. In this case, the roughness elements of the body and to some degree the inhomogeneities play a significant role in the scattering.

While carrying out this analysis, an artefact of the predictions involving modelling of the high resolution features was discovered (introduction of facets that caused unrealistic scattering levels). Although the difficulty was resolved by use of a smoothing operation, the artefact illustrated the great care one must take in attempting to increase the resolution and accuracy of the predictions. Certainly, use of a full three-dimensional model of the animal may have prevented this particular artefact from arising. However, digitizing all shape and material properties is sufficiently challenging that it is conceivable that artefacts can arise due to the inherent inaccuracies of the measurement process.

In conclusion, a significant effort is required for the development of a model that accurately predicts the acoustic scattering over a wide range of conditions. The study presented here for euphausiids and copepods suggests that high-resolution models provide accuracy over a wide range of conditions. While such complex models were shown to be essential for some conditions, they were not necessary for others. For practical considerations in any modelling effort, the model should be no more complex than the conditions warrant.

Acknowledgements

The authors are grateful to Phil Alatalo of the Biology Department, Woods Hole Oceanographic Institution (WHOI), Woods Hole, MA for supplying the copepods for the experiment, Shirley Barkley and Sheila Hurst of the Department of Applied Ocean Physics and Engineering (WHOI) for preparing the manuscript to this paper, and Jack Cook and Jayne Doucette of Graphics (WHOI) for drawing some of the figures. This research was supported by the US Office of Naval Research Grant No. N00014-95-1-0287. This is WHOI contribution No. 9927.

References

Anderson, V. C. 1950. Sound scattering from a fluid sphere. Journal of the Acoustical Society of America, 22: 426–431.

Benfield, M. C., Davis, C. S., and Gallager, S. M. 2000. Estimating the *in situ* orientation of *Calanus finmarchicus* on Georges Bank using the Video Plankton Recorder. Plankton Biology and Ecology 47(1): 69–72.

Chu, D., Stanton, T. K., and Wiebe, P. H. 1992. Frequency dependence of sound backscattering from live individual zooplankton. ICES Journal of Marine Science, 49: 97–106.

Chu, D., Foote, K. G., and Stanton, T. K. 1993. Further analysis of target strength measurements of Antarctic krill at 38 and 120 kHz: Comparison with deformed cylinder model and inference of orientation distribution. Journal of the Acoustical Society of America, 93: 2985–2988.

Cochrane, N. A., Sameoto, D. D., and Belliveau, D. J. 1994. Temporal variability of euphausiid concentrations in a Nova Scotia shelf basin using a bottom-mounted acoustic Doppler current profiler. Marine Ecology Progress Series, 107: 55–66.

Endo, Y. 1993. Orientation of Antarctic Krill in an aquarium. Nippon Suisan Gakkaishi, 59: 465–468.

Foote, K. G. 1990. Speed of sound in *Euphausia superba*. Journal of the Acoustical Society of America, 87: 1405–1408.

Foote, K. G. 1998. Broadband acoustic scattering signatures of fish and zooplankton (project BASS). Proceedings of the Third European Marine Science and Technology Conference, Lisbon, May 23–27, 3: 1011–1025.

Foote, K. G., Everson, I., Watkins, J. L., and Bone, D. G. 1990. Target strengths of Antarctic krill (*Euphausia superba*) at 38 and 120 kHz. Journal of the Acoustical Society of America, 87: 16–24.

Francis, D. T. I., Oswin, J. R., and Macey, P. C. 1996. Comparing FE/BE models with measurement: flextensional transducers. Proceedings of the Institute of Acoustics, 18(10): 31–40.

Greenlaw, C. F. 1977. Backscattering spectra of preserved zooplankton. Journal of the Acoustical Society of America, 62: 44–52.

Greenlaw, C. F. 1979. Acoustical estimation of zooplankton populations. Limnol. Oceanogr., 24: 226–242.

Holliday, D. V., Pieper, R. E., and Kleppel, G. S. 1989. Determination of zooplankton size and distribution with multi-frequency acoustic technology. Journal du Conseil International pour L'Exploration de la Mer, 46: 52–61.

Holliday, D. V., and Pieper, R. E. 1995. Bioacoustical oceanography at high frequencies. ICES Journal of Marine Science, 52: 279–296.

Johnson, R. K. 1977. Sound scattering from a fluid sphere revisited. Journal of the Acoustical Society of America, 62: 375–377; "Erratum: 'Sound scattering from a fluid sphere revisited'." Journal of the Acoustical Society of America, 63, 626 (1978).

Johnson, M. L. 1993. Orientation dependence of the acoustic backscatter for elongated zooplankton. Ocean Engineer Thesis, Massachusetts Institute of Technology/Woods Hole Oceanographic Institution.

Kils, U. 1981. The swimming behavior, swimming performance and energy balance of Antarctic krill, Euphausia superba. BIOMASS Science Series Vol. 3.

Kristensen, Å., and Dalen, J. 1986. Acoustic estimation of size distribution and abundance of zooplankton. Journal of the Acoustical Society of America, 80: 601–611.

Martin, L. V., Stanton, T. K., Lynch, J. F., and Wiebe, P. H. 1996. Acoustic classification of zooplankton. ICES Journal of Marine Science, 53: 217–224.

Martin Traykovski, L. V., Stanton, T. K., Wiebe, P. H., and Lynch, J. F. 1998a. Model-based covariance mean variance classification techniques: Algorithm development and application to the acoustic classification of zooplankton. IEEE Journal of Oceanic Engineering, 23: 344–364.

Martin Traykovski, L. V., O'Driscoll, R. L., and McGehee, D. E. 1998b. Effect of orientation on broadband acoustic scattering of Antarctic krill *Euphausia superba*: Implications for inverting zooplankton spectral acoustic signatures for angle of orientation. Journal of the Acoustical Society of America, 104: 2121–2135.

McGehee, D. E., O'Driscoll, R. L., and Martin-Traykovski, L. V. 1998. Effects of orientation on acoustic scattering for Antarctic krill at 120 kHz. Deep Sea Research II, 45: 1273–1294.

Medwin, H., and Clay, C. S. 1998. Fundamentals of Acoustical Oceanography. Academic Press, Boston. 712 pp.

Miyashita, K., Aoki, I., and Inagaki, T. 1996. Swimming behavior and target strength of isada krill (*Euphausia pacifica*). ICES Journal of Marine Science, 53: 303–308.

Morse, P. M., and Ingard, K. U. 1968. Theoretical Acoustics. Princeton University Press, Princeton, NJ. Chap. 8.

Partridge, C., and Smith, E. R. 1995. Acoustic scattering from bodies: Range of validity of the deformed cylinder method. Journal of the Acoustical Society of America, 97: 784–795.

Samovolkin, V. G. 1980. Backscattering of ultrasonic waves by shrimps. Oceanology, 20: 1015–1020.

Sars, G. O. 1903. An account of the Crustacea of Norway. The Bergen Museum, Bergen.

Stanton, T. K. 1988. Sound scattering by cylinders of finite length I: Fluid cylinders. Journal of the Acoustical Society of America, 83: 55–63.

Stanton, T. K. 1989a. Sound scattering by cylinders of finite length III: Deformed cylinders. Journal of the Acoustical Society of America, 86: 691–705.

Stanton, T. K. 1989b. Simple approximate formulas for backscattering of sound by spherical and elongated objects. Journal of the Acoustical Society of America, 86: 1499–1510.

Stanton, T. K., Nash, R. D. M., Eastwood, R. L., and Nero, R. W. 1987. A field examination of acoustical scattering from marine organisms at 70 kHz. IEEE Journal of Oceanic Engineering, OE-12: 339–348.

Stanton, T. K., Clay, C. S., and Chu, D. 1993a. Ray representation of sound scattering by weakly scattering deformed fluid cylinders: Simple physics and application to zooplankton. Journal of the Acoustical Society of America, 94: 3454–3462.

Stanton, T. K., Chu, D., Wiebe, P. H., and Clay, C. S. 1993b. Average echoes from randomly oriented random-length finite cylinders: Zooplankton models. Journal of the Acoustical Society of America, 94: 3463–3472.

Stanton, T. K., Wiebe, P. H., Chu, D., Benfield, M., Scanlon, L., Martin, L., and Eastwood, R. L. 1994a. On acoustic estimates of zooplankton biomass. ICES Journal of Marine Science, 51: 505–512.

Stanton, T. K., Wiebe, P. H., Chu, D., and Goodman, L. 1994b. Acoustic characterization and discrimination of marine zooplankton and turbulence. ICES Journal of Marine Science, 51: 469–479.

Stanton, T. K., Chu, D., and Wiebe, P. H. 1996. Acoustic scattering characteristics of several zooplankton groups. ICES Journal of Marine Science, 53: 289–295.

Stanton, T. K., Chu, D., and Wiebe, P. H. 1998a. Sound scattering by several zooplankton groups. II. Scattering models. Journal of the Acoustical Society of America, 103: 236–253.

Stanton, T. K., Wiebe, P. H., and Chu, D. 1998b. Differences between sound scattering by weakly scattering spheres and finite length cylinders with applications to sound scattering by zooplankton. Journal of the Acoustical Society of America, 103: 254–253.

Urick, R. J. 1983. Principles of Underwater Sound. McGraw-Hill, New York.

Wiebe, P. H. 1976. The biology of cold-core rings. Oceanus, 19: 69–76.

Wiebe, P. H., Greene, C. H., Stanton, T. K., and Burczynski, J. 1990. Sound scattering by live zooplankton and micronekton: Empirical studies with a dual-beam acoustical system. Journal of the Acoustical Society of America, 88: 2346–2360.

Wiebe, P. H., Mountain, D. G., Stanton, T. K., Greene, C. H., Lough, G., Kaartvedt, S., Dawson, J., and Copley, N. 1996. Acoustical study of the spatial distribution of plankton on Georges Bank and the relationship between volume backscattering strength and the taxonomic composition of the plankton. Deep-Sea Research II, 43: 1971–2001.

Yayanos, A. A., Benson, A. A., and Nevenzel, J. C. 1978. The pressure-volume-temperature (PVT) properties of a lipid mixture from a marine copepod, *Calanus plumchrus*: implications for buoyancy and sound scattering. Deep-Sea Research, 25: 257–268.